Volume 18
Number 42
14 November 2022
Pages 8055–8204

Soft Matter

rsc.li/soft-matter-journal

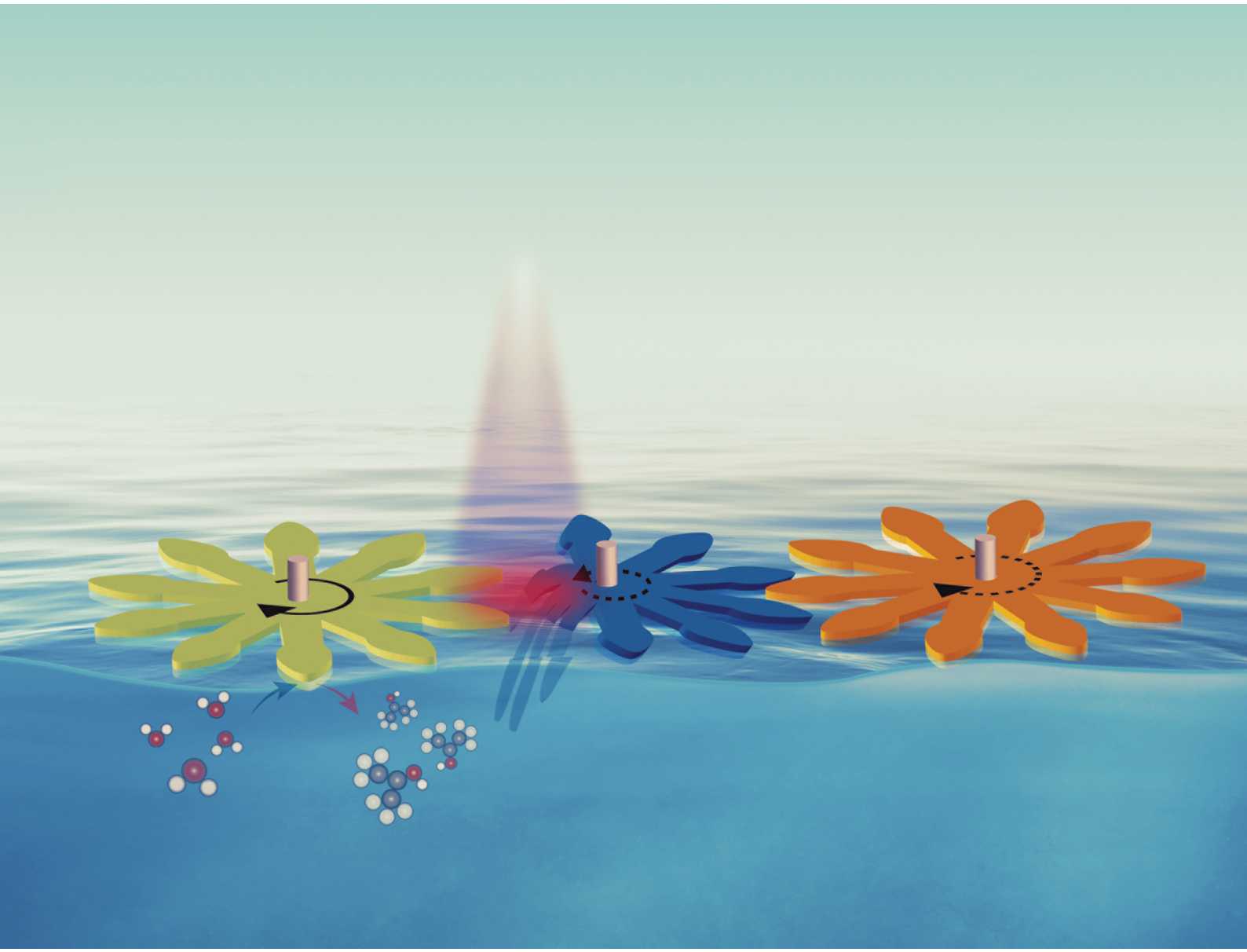

ISSN 1744-6848

ROYAL SOCIETY OF CHEMISTRY

PAPER

Abdon Pena-Francesch, Hamed Shahsavan *et al.*
Plasticized liquid crystal networks and chemical motors for the active control of power transmission in mechanical devices

Soft Matter

PAPER

View Article Online
View Journal | View Issue

Cite this: *Soft Matter*, 2022, 18, 8063

Plasticized liquid crystal networks and chemical motors for the active control of power transmission in mechanical devices†

Natalie P. Pinchin,‡[a] Chia-Heng Lin,‡[b] Cecelia A. Kinane,[b] Naoki Yamada,[c] Abdon Pena-Francesch *[b] and Hamed Shahsavan *[a]

Received 21st June 2022,
Accepted 8th August 2022

DOI: 10.1039/d2sm00826b

rsc.li/soft-matter-journal

The miniaturization of mechanical devices poses new challenges in powering, actuation, and control since traditional approaches cannot be used due to inherent size limitations. This is particularly challenging in untethered small-scale machines where independent actuation of multicomponent and multifunctional complex systems is required. This work showcases the integration of self-powered chemical motors and liquid crystal networks into a powertrain transmission device to achieve orthogonal untethered actuation for power and control. Driving gears with a protein-based chemical motor were used to power the transmission system with Marangoni propulsive forces, while photothermal liquid crystal networks were used as a photoresponsive clutch to engage/disengage the gear system. Liquid crystal networks were plasticized for optimized photothermal bending actuation to break the surface tension of water and achieve reversible immersion/resurfacing at the air–water interface. This concept is demonstrated in a milliscale transmission gear system and offers potential solutions for aquatic soft robots whose powering and control mechanisms must be necessarily decoupled.

Introduction

Over the past two decades, there has been growing interest across research fields in the development of small-scale machines and devices (ranging from several millimeters to a few micrometers) for applications in electronics, sensing, bioengineering, environmental science, and robotics.[1–5] Due to inherent size limitations, traditional power and control methods that require voluminous components cannot be incorporated into small-scale machine designs. Therefore, there is a need for alternative powering, navigating, functioning, and control strategies that can be utilized at smaller scales.[6] Untethered machines are of particular interest as they can be autonomously powered and remotely controlled without requiring cables, pumps, or other external connections, which impose constraints on use in certain environments.[7–9] To power such untethered machines, a variety of energy sources have been developed, including magnetic fields,[10–12] light,[13–16] acoustic fields,[17–19] electric fields,[20] and chemical energy.[21,22] However, the active control function in such small-scale systems is a challenging task, especially when selective control of multicomponent systems is desired.

To achieve selective actuation of multiple components or multiple functions, one can combine powering and control mechanisms of orthogonal nature, such as chemically-driven propulsion for powering and stimuli-responsive actuation for control, for decoupling each function. Self-powered mechanisms such as chemical motors are of particular interest due to the fact that they can operate autonomously by consuming onboard or in-media chemical fuel. Among these, Marangoni motors are a popular choice for locomotion at the air–water interface. This motor mechanism (inspired by the locomotion of semiaquatic insects)[23] relies on propulsive forces generated by anisotropic surface tension gradients,[24] and it has been exploited to propel robotic platforms locomoting on the surface of water.[21,25] Many approaches in developing Marangoni-propelled systems hinge on chemical fuels added at the air–water interface or trapped and released from a motor matrix. These motors have evolved from microdroplets[26] to systems using organic matrices[21,27,28] and fluid reservoirs[25,29] with greater capacity for fuel storage. While these systems usually present control and efficiency challenges, they can provide

[a] *Department of Chemical Engineering, Waterloo Institute for Nanotechnology, University of Waterloo, Waterloo, ON, N2L 3G1, Canada. E-mail: hshahsav@uwaterloo.ca*
[b] *Department of Materials Science and Engineering, Macromolecular Science and Engineering, Robotics Institute, University of Michigan, Ann Arbor, MI, 48109, USA. E-mail: abdon@umich.edu*
[c] *Department of System Innovation, Osaka University, Osaka, 560-0043, Japan*

† Electronic supplementary information (ESI) available. See DOI: https://doi.org/10.1039/d2sm00826b

‡ N.P.P. and C.L contributed equally to this work.

sustained propulsion over long periods of time without the need for continuous external stimuli.

Stimuli-responsive cross-linked networks of liquid crystal polymers (LCNs) offer interesting solutions for the control of robotic systems by inducing localized actuation. LCNs are an attractive class of molecularly anisotropic materials with stimuli responsiveness. External stimuli, such as heat or light temporarily disrupt the anisotropic molecular order, known as the director field (n), thereby creating internal stresses and anisotropic bulk deformation. The local LCN director field can be preprogrammed to create complex shape changes when actuated.[30] The sensitivity of these materials to a variety of cues, such as light and temperature, and their shape-change programmability, through different molecular alignment methods, have triggered a great body of research about their applications in soft-robotics.[4,5,31–36] The majority of reported LCN systems rely on direct heat or photothermal heat generation for actuation. However, these methods typically have lower energy conversion efficiency due to the large energy loss or dissipation to the surroundings. The actuation is even less efficient, and consequently slower, under or at the surface of the water which has a high overall coefficient of heat transfer. As demonstrated in previous work, the addition of a nematogenic solvent to the LCN can sharpen the nematic to isotropic transition temperature (T_{NI}), decrease the energy required for the actuation, and enhance the actuation efficiency to a point where the system can change its shape underwater.[37] For a similar reason, the photothermal actuation of LCNs plasticized with short-chain nematogenic solvents (PLCN) was selected for this work for achieving large deformations in wet conditions.

In this work, we present a showcase for the orthogonal use of protein motors and shape morphing LCNs for untethered powering and control of a multi-component mechanical device. We designed and fabricated a milli-scale powertrain transmission with active gears that integrate motor and clutch functionalities into the device (Fig. 1). The active driving gear uses Marangoni propulsive forces at the air–liquid interface generated by onboard protein motors.[21] The active clutch gear uses photothermal actuation of PLCNs to bend the gear teeth and disengage from the gear train,[37] breaking the transmission across the gear train. While Marangoni self-powered motors and untethered control of LCNs have previously been studied separately, the integration of the two mechanisms allows for simultaneous powering of the gear train and orthogonal untethered control of the transmission, which offers new design and control possibilities for multicomponent and multifunctional mechanical devices and soft micromachines.

Results and discussion

Protein motors for power generation

To power the gear train, we applied a functional motor coating to an initially inactive gear and used it as the driving gear in our transmission system. The motors are based on Marangoni propulsion achieved by the release of hexafluoroisopropanol (HFIP) stored in squid sucker ring teeth (SRT) proteins.[21] HFIP is a volatile low surface tension solvent that is used as a chemical fuel entrapped in an SRT protein motor matrix,[38] which is composed of semicrystalline polypeptides found in suction cups on the tentacles and arms of squids.[39,40] SRT proteins can be dissolved in HFIP, resulting in a motor-and-fuel complex solution that can be applied as a coating to a broad range of substrates and materials (in this case, the teeth of the driving gear, Fig. 2a).[41,42] After evaporation of the solvent, residual fuel remains infused in the SRT protein coating. As the coating comes in contact with water the fuel molecules infused in the protein matrix diffuse into the liquid media and lower the local surface tension.

We fabricated a module 1 (m1) gear set with 10, 20, and 30 teeth (z10, z20, and z30 respectively) (Fig. 2b) and applied the protein motor coating to the teeth. The gears were designed with a modified extended teeth profile to increase the cantilever length and facilitate fuel release and the clutch function. By selectively coating one side of each tooth, we can create an anisotropic surface tension gradient around the gear tooth that

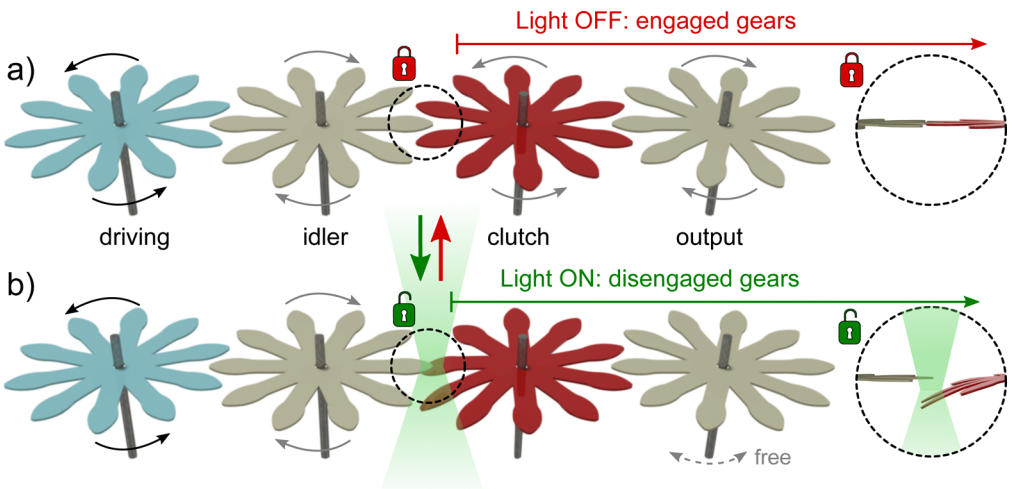

Fig. 1 Concept of the powertrain transmission consisting in a gear train with active gears. The driving gear powers the gear train *via* onboard chemical motors. The clutch gear, fabricated from PLCNs, is photothermally activated to (a) engage and (b) disengage from the gear train.

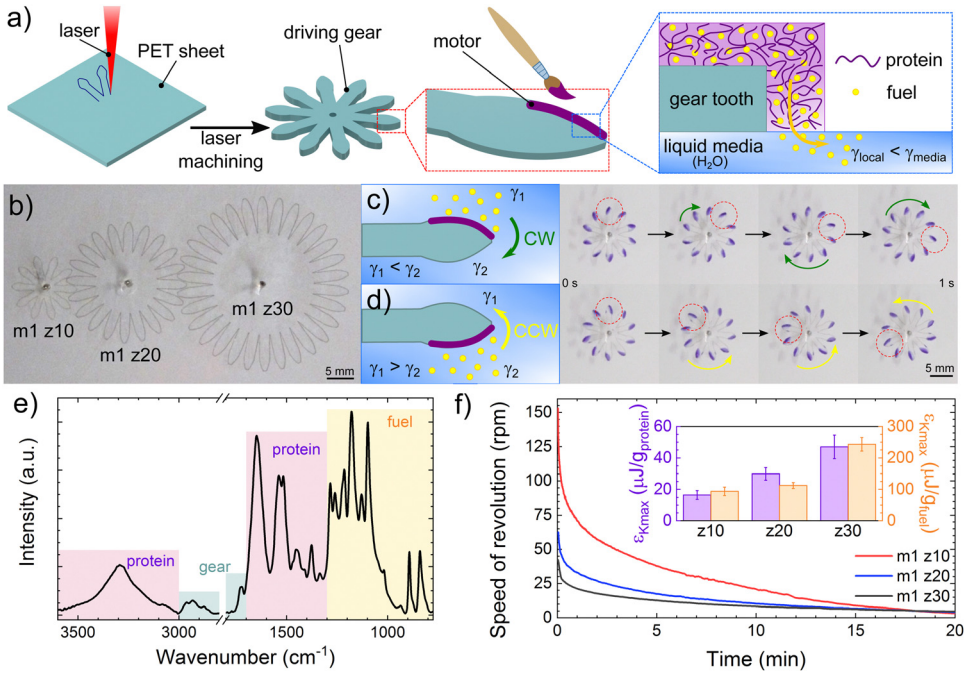

Fig. 2 Protein motors. (a) Fabrication of the driving gear by laser micromachining of PET thin sheets and application of functional motor coating consisting of chemical fuel entrapped in a protein matrix; (b) m1 gear set, with number of teeth z10, z20, and z30; (c) clockwise (CW) and (d) counterclockwise (CCW) motion of the driving gear by selective motor coating application on either side of the teeth; (e) chemical analysis of motors in driving gear by FTIR; (f) rotational speed, specific work, and fuel efficiency of m1 driving gears (z10, z20, and z30).

generates a Marangoni propulsive force towards high surface tension. This results in the Marangoni-driven rotation of an active gear rotating on a fixed axle, which constrains translational motion and enforces rotation. We can preprogram rotational motion in clockwise (CW) or counterclockwise (CCW) directions by selectively coating either side of the gear teeth (Fig. 2c and d, and ESI† Movie S1), and the fuel can be reapplied as needed. Fourier Transform Infrared (FTIR) spectroscopy analysis of the motor-coated gear teeth showed characteristic absorption bands from the protein (amide I, amide II, amide A), fuel (1100–1300 cm^{-1}), and the polymer substrate (polyethylene terephthalate PET film, 1700–1800 cm^{-1}, 2800–300 cm^{-1}), which indicates that the protein motors are successfully integrated with the gear teeth while conserving the infused fuel (Fig. 2e). The motor coating can propel the gears with rotational velocities up to 150, 47, and 45 rpm for z10, z20, and z30 teeth, respectively. As the fuel is released into the water surface and is progressively depleted from the motor matrix, the velocity decreases accordingly due to a lower local concentration of chemical fuel at the interface. The specific work of the motor $\varepsilon_{K_{max}}$, defined as the maximum rotational kinetic energy ($I\omega^2/2$, where I is the moment of inertia around the axis and ω is the angular velocity) per motor weight (protein mass), and fuel efficiency (kinetic energy per gram of fuel) can reach up to 47 μJ $g_{protein}^{-1}$ and 243 μJ g_{fuel}^{-1} (Fig. 2f). Due to the high efficiency of these motors,[21] the gear train can be powered with very small amounts of fuel and operate for prolonged periods of time with a single coating application (up to 20 minutes), which makes the material very attractive as a modular power source for the driving gear.

Liquid crystal network clutch fabrication

To design and fabricate a stimuli-responsive active clutch gear, we chose acrylate-based glassy liquid crystal networks due to their propensity for accurate, yet straightforward molecular alignment. The selected liquid crystal networks are aligned using photoalignment; a powerful tool for the precise alignment of liquid crystals due to its accuracy and versatility.[34] Complex alignment patterns can be achieved using linearly polarized light and patterned photomasks.[43] As shown in Fig. 3a, the LCN is composed of a mesogenic diacrylate monomer as a cross-linker (M1: 7.7 mol%), side-chain mesogenic mono-acrylate monomers that form the backbone (M2: 90.3 mol%), and mono-acrylate photo-chromophore molecules (DR1A: 1 mol%) for photothermal local heat generation. Irgacure 651 (1 mol%) was used as the photoinitiator. According to our design in Fig. 1, the gear teeth on the LC-based clutch must be able to undergo reversible and on-demand bending actuation. We can achieve such a shape-change by a splay alignment of mesogens through the thickness of an LC-based construct. As shown in Fig. 3b, a splay LCN film exposed to photothermal heating bends due to expansion on the side with homeotropic alignment, and shrinkage on the opposing side with planar alignment. In order to render a similar shape-change behavior on the teeth of the LCN clutch gears, we aligned the mesogens on one side of the film radially and aligned them homeotropically on the other side. Fig. 3c shows a schematic view of the LCN gear fabrication process through the conventional capillary filling of an empty glass cell. We chose a photoalignment technique to induce in-plane radial orientation of mesogens adjacent to one side of the cell. For this, we

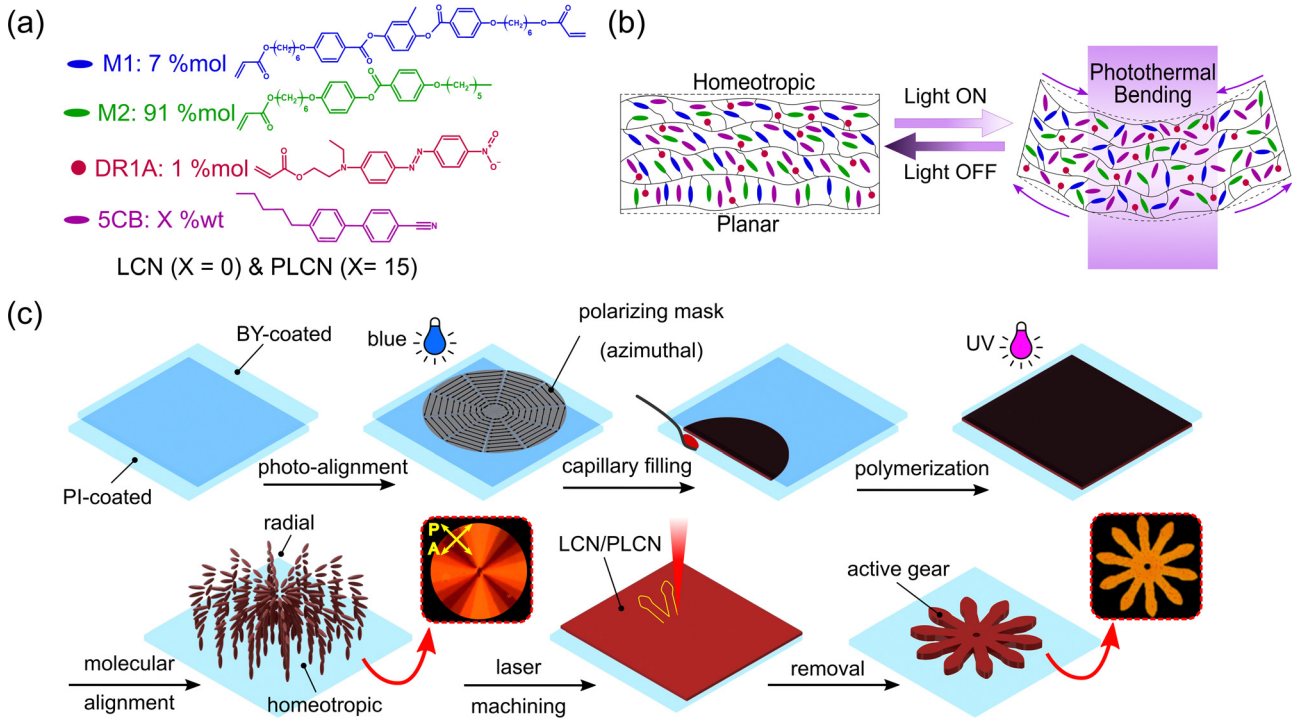

Fig. 3 (a) Molecular structure of constituent molecules in LCN and PLCN; (b) mechanism of photothermal bending deformation in LC-based cross-linked networks; (c) fabrication schematic view of the LCN gears fabrication with pre-determined molecular alignment. Molecules are aligned radially adjacent to the side of the cell that is exposed to polarized light. Molecules are aligned homeotropically on the other side of the film.

spin-coated a glass substrate with a brilliant yellow and dimethylformamide (BY-DMF) solution, baked it at 90 °C, and exposed the substrate to blue light ($\lambda \sim 447$ nm) through a polarization mask. Our polarization mask was made of multiple polarizers cut into wedges using a laser micromachining tool. They were then assembled manually on a glass substrate to form a circular mask with azimuthal polarization (Fig. 3c). The BY molecules exposed to the light with azimuthal polarization

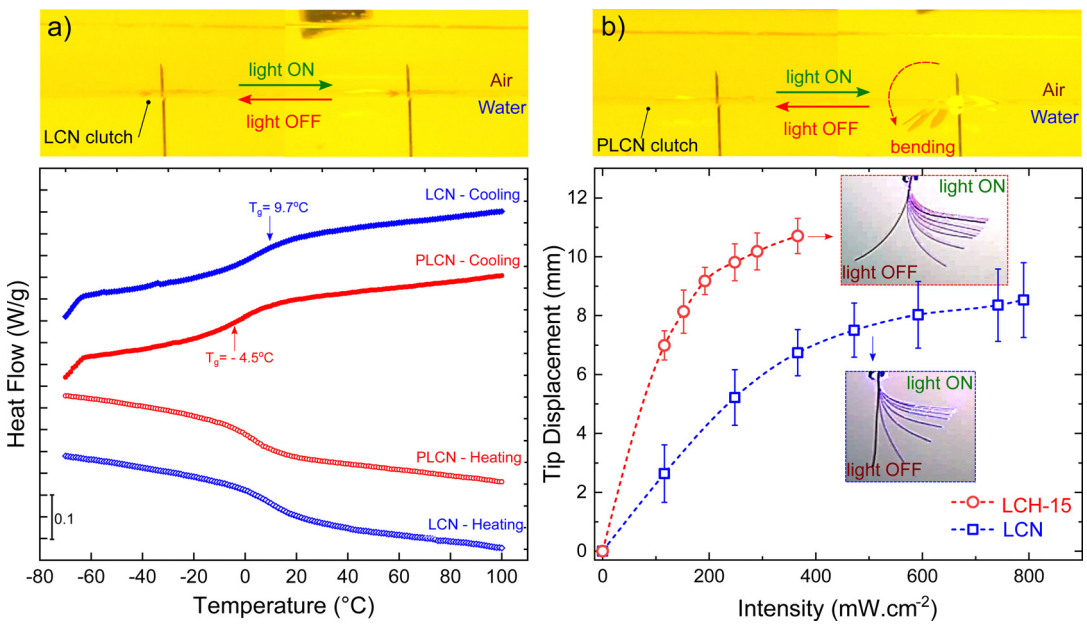

Fig. 4 (a) Exposing LCN gears to light with high intensities did not lead to a discernable shape change and eventual breaking of the capillary bridge; (b) DSC results from −70 to 100 shows the largea shift of the glass transition temperature by adding 15 wt% 5CB to the LCN original mixture; (c) PLCN gear underwent a drastic shape change with even lower energy input due to the lower Tg and stiffness, breaking the surface tension and submerging in water; (d) the difference between the photothermal Photothermal deformation of LCN and PLCN cantilevers in air.

render an orthogonal LC molecular alignment. The homeotropic molecular alignment on the opposing side was achieved by coating the substrate with polyimide. After cross-linking of the LC mixture by UV, a typical fan texture of the transmitted light through the fabricated film between crossed polarizers confirmed the successful radial alignment of the mesogens. The cross-linked film with radial and homeotropic molecular alignment on opposing sides was then laser micromachined into the desired gear shape. Afterward, the gear was suspended on the air–liquid interface for further experiments.

Liquid crystal network clutch characterization

Initial experiments on the photothermal actuation of LCN gears at the air–liquid interface did not result in a discernible shape-change of gear teeth as desired (Fig. 4a). We postulate that the photothermal actuation of our LCN gear is hindered mainly due to the extensive dissipation of generated heat from the bottom side that is exposed to the water. Consequently, the bending actuation of the gear teeth is not large enough to overcome the capillary forces acting on them. It has been recently shown, in a similar scenario, that the energy conversion efficiency and thermal actuation of photothermal LCNs dramatically decrease when they are immersed in water.[37] Such a reduction was partly attributed to the extensive dissipation of generated heat inside water, and partly to the drag force acting on the LCN construct.[37] Plasticizing the original LCN network by adding a certain amount of low molecular weight liquid crystal molecules, such as 5CB, was proposed as a solution to alleviate this problem. We added 15 wt% 5CB to the LCN precursor to plasticize the network and facilitate its photothermal deformation at the air–liquid interface. Our initial assessment of the thermo-physical properties using differential scanning calorimetry (DSC) showed that the glass transition temperature (T_g) of the plasticized LCN (PLCN) is greatly reduced compared to that of its LCN counterpart. Fig. 4b shows the results of the second thermal cycle after erasing the thermal memory of the samples in the first cycle. Both samples do not show an appreciable nematic-to-isotropic transition, which is expected due to the supercritical nature of phase transition for this class of glassy networks.[44] For this class of materials, shape change occurs gradually as the LCNs are heated beyond their T_g. The glass transition temperature of the PLCN ($T_g \approx -4.5$ °C) is reduced compared to that of the original LCN ($T_g \approx 9.5$ °C), which widens the thermal actuation window by almost 14 °C. In previous work, it was observed that LCNs become remarkably softer by the addition of a nematogenic solvent to their precursor.[37] We anticipate higher energy conversion efficiency as a result of the decrease in the T_g and stiffness. Indeed, the plasticization of the LCN resulted in more efficient photothermal actuation of gear teeth, allowing the gear to break the surface tension and submerge in water by bending (Fig. 4c and ESI† Movie S2). The photothermal actuation of splay cantilevers in air, shown in Fig. 4d, demonstrates the great improvement of bending *vs.* light intensity for PLCN samples. Initially, the clutch gear was positioned such that the teeth would actuate upwards into the air to disengage from the neighboring gear (homeotropic side facing the water). However, the PLCN was unable to overcome the surface tension and elastocapillary forces acting upon it. As such, the configuration was modified so the teeth would instead actuate downwards into the water (homeotropic side facing air). The PLCN is not hydrophobic, as determined by its contact angle with water ($<90°$), so the elastocapillary force is pulling it downwards. By actuating into the water the PLCN moves with the elastocapillary force rather than against it, and is able to successfully break the surface tension and actuate into the water.

Orthogonal actuation of a hybrid gear train mechanical device

To demonstrate the active control of power transmission by the two orthogonal signals of chemical energy and light, we

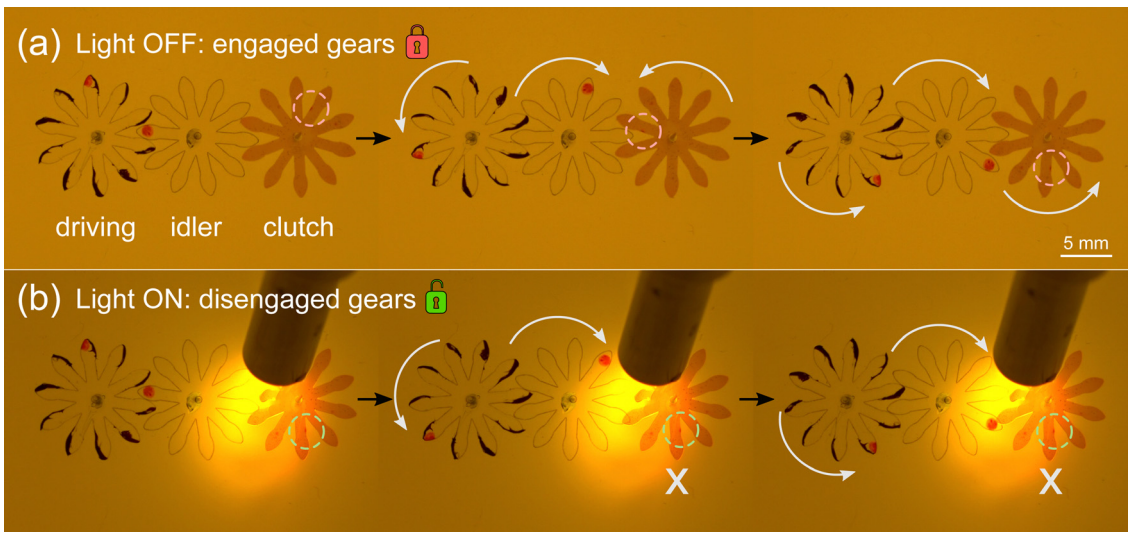

Fig. 5 Power transmission through a gear train system with active gears (self-propelled driving gear and a liquid crystal network clutch). (a) Without light, gears are engaged and power is transmitted throughout the gear train. (b) When illuminated, the active PLNC gear deforms and disengages from the gear train, interrupting power transmission (X) and effectively acting as a clutch mechanism.

integrated active gears into a milli-scale proof-of-concept gear train (Fig. 5). The gear train consists of the (i) driving gear (with a chemical motor coating), (ii) idler gear, and (iii) clutch gear (PLCN). The driving gear was selectively coated with protein motors to generate Marangoni propulsive forces as previously discussed. The protein motors, visible in dark violet color, were selectively applied on one side of the gear teeth only, inducing counterclockwise (CCW) rotation on the driving gear. The rotational motion is transmitted to the adjacent idler gear (CW), and then to the clutch gear (CCW), which can be observed by tracking marks on the surface of the gear teeth. When the light is off (Fig. 5a), the PLCN gear remains inactive and preserves its initial conformation (*i.e.*, flat, non-deformed), locking with the gear train and receiving power (engaged). When the light is on (Fig. 5b), the illuminated PLCN gear teeth bend downwards (submerged) to interrupt the power transmission (while the driving and idle gears are moving, the clutch gear does not). PLCNs offer fast gear teeth actuation at low temperatures while producing enough work to break the surface tension of the air–liquid interface and submerge underwater. This actuation of PLCN teeth results in the disengagement of the gear from the mechanical device, effectively acting as a clutch mechanism: power transmission throughout the gear train is interrupted on-demand, while the rest of the components remain free to move (and ESI† Movie S3). If the light stimulus is not applied directly to the desired teeth only, accidental flood illumination may occur, which will increase the temperature of the surrounding water. As the surface tension of water decreases with temperature, excess illumination outside of the clutch teeth might slow down (and even "stall") the gear train due to thermocapillary convection competing with the Marangoni propulsion. The reversible engagement/disengagement of the gear train is demonstrated in a four gear power transmission device (ESI† Movie S4). This device is composed of a m1 z30 driving gear, two m1 z10 idlers, and a m1 z10 PLCN active clutch gear. Upon exposure to light, the clutch tooth starts bending and slides under the inactive tooth, thus disengaging from the idler and allowing its free rotation. When the UV light stimulus is off, the PLCN clutch relaxes back to its initial flat state, engaging back with the gear train through the alignment of its teeth with the neighboring idler gear. This provides a reversible mechanism to control the power transmission through the gear train device on demand.

Conclusions

A milliscale gear train power transmission is used to showcase the use of protein chemical motors and PLCNs for untethered powering and control, respectively, for small-scale multicomponent mechanical devices. The driving gear containing chemical motors provides power to the system, while the PLCN gear acts as a clutch, disengaging and halting the power transmission through the gear train when illuminated. The driving gear is powered by Marangoni propulsion forces generated by functional motor coatings applied to the driving gear teeth. These motor coatings are composed of a structural protein matrix infused with low surface tension chemical fuel that is released at the air–water interface (thus generating Marangoni flows). These motor protein-fuel complexes can propel a set of gears with high efficiency for prolonged periods of time with a single coating application, effectively acting as the main power source for the mechanical device. In parallel, the clutch gear is composed of plasticized liquid crystal networks with increased energy conversion efficiency and reduced T_g for optimized photothermal bending actuation. The combination of these Marangoni protein motors and photothermal LCNs provides an orthogonal untethered actuation method for selective control of the functions of mechanical devices (in this case, a small-scale power transmission). Such hybrid systems will offer new actuation, powering, and control strategies for multicomponent and multifunctional small-scale devices with potential solutions to the miniaturization challenges of untethered mechanical micromachines.

Experimental section

Materials

Bi-functional monomer 1,4-bis-[4-(6-acryloyloxyhexyloxy) benzoyloxy]-2-methylbenzene (M1), mono-functional monomer 4-(6-acryloxy-hex-1-yl-oxy)-phenyl 4-(hexyloxy)-benzoate (M2), and low molecular weight non-reactive liquid crystal 4-cyano-4′-*n*-pentylbiphenyl (5CB) were purchased from SYNTHON Chemicals GmbH & Co. KG. Dispersed red 1 acrylate (DR1A), 2,2-dimethoxy-2-phenylacetophenone (Irgacure®651) *N*,*N*-dimethylformamide (DMF), 1,1,1,3,3,3-hexafluoro-2-propanol (HFIP), and crystal violet dye were purchased from Sigma-Aldrich. Brilliant yellow (BY) was purchased from TCI. Polyimide SE-1211 was donated by Nissan Chemical Industries. All reagents and solvents were used as received without further purification. Squid sucker ring teeth (SRT) proteins were extracted from Loligo Vulgaris squid species and purified as described elsewhere.[39]

Gear train fabrication

The driving and idler gears were fabricated from polyethylene terephthalate (PET) films (100 μm thick). The PET films were laser-micromachined to the desired gear design (modified m1 z10, z20, z30 gears). G21 syringe needles were adhered to the bottom of a polystyrene Petri dish and served as vertical axles. The Petri dish was filled with deionized water and the gears were assembled floating at the air–liquid interface. The driving gear was partially coated on the edges of its teeth with a solution of purified SRT protein dissolved in hexafluoroisopropanol (HFIP) at a concentration of 50 mg mL^{-1} (with an additional 1% crystal violet dye for visualization). Coated gears were dried in a fume hood for 1 h. Finally, the performance of the motors and the gear train was recorded with a Sony HDR camera (25 fps), and velocities were analyzed in MATLAB with a custom particle-tracking code.

Fabrication and characterization of LC-based gears

We fabricated LCN films by injecting a mixture of M1 and M2 monomers into capillary cells (100 μm gap) with predetermined molecular alignment at temperatures higher than the mixture clearing point (T_{NI}). The mixture was cooled down to its nematic mesophase at 30 °C ($< T_{NI}$); afterward, it was cross-linked by photo-polymerization using UV light. We made plasticized LCNs (PLCNs) by adding 15 wt% 5CB to the initial mixture. LCN and PLCN films were micromachined to the desired gear shape using an LPKF ProtoLaser U3 laser cutter (3.5 W, 54 kHz). We have elaborated on the details of the fabrication and molecular alignment procedures in Section 2.2. The assembly of the fabricated LCN and PLCN gears into the gear train was similar to the process stated in the section above.

Materials characterization

Glass transition and nematic-to-isotropic temperatures (T_g, and T_{NI}) of the polymerized LCN and PLCN films were measured by differential scanning calorimetry (DSC) using a DSC2500 from TA Instruments. We monitored the variation of heat flux with temperature for LCN and PLCN samples between −80 °C and 150 °C in two consecutive cycles (10 °C min^{-1}). Driving gears were analyzed by Fourier Transform Infrared (FTIR) spectroscopy in a ThermoFisher Nicolet iS20 spectrometer with an Attenuated Total Reflection accessory at 128 scans and 4 cm^{-1} resolution per spectrum.

Actuation characterization

To estimate the photothermal actuation of LCN and PLCN gear teeth, we used LCN and PLCN cantilevers with splay alignment. The length of each cantilever was set to 6 mm, corresponding to the length of each gear tooth from its tip to the center of the gear. One-end fixed cantilevers were exposed to light from a high-pressure mercury vapor short arc UV lamp (Omnicure S2000, Excelitas Technologies) with distinctive peaks in the UV-vis region (300 nm to 600 nm). The tip displacement *vs.* light intensity was monitored by a digital microscope (Dino-lite) and measured manually using the Fiji image-processing package.

Author contributions

A. P. F and H. S. conceived, designed, and supervised the project. N. P. P., C. H. L., C. K. A., and N. Y. performed the experiments and analysis of data. N. P. P., C. A. K., A. P. F., and H. S. wrote the manuscript, and all authors agreed with its contents.

Conflicts of interest

There are no conflicts to declare.

Acknowledgements

This project was supported by the Natural Sciences and Engineering Research Council of Canada (NSERC) and partially supported by the American Chemical Society Petroleum Research Fund (ACS PRF).

Notes and references

1 M. Li, A. Pal, A. Aghakhani, A. Pena-Francesch and M. Sitti, Soft actuators for real-world applications, *Nat. Rev. Mater.*, 2022, **7**(3), 235–249.
2 L. Hines, K. Petersen, G. Z. Lum and M. Sitti, Soft Actuators for Small-Scale Robotics, *Adv. Mater.*, 2017, **29**(13), 1603483.
3 J. Li, B. Esteban-Fernández de Ávila, W. Gao, L. Zhang and J. Wang, Micro/nanorobots for biomedicine: Delivery, surgery, sensing, and detoxification, *Sci. Robot.*, 2017, **2**(4), eaam6431.
4 C. Ahn, X. Liang and S. Cai, Bioinspired Design of Light-Powered Crawling, Squeezing, and Jumping Untethered Soft Robot, *Adv. Mater. Technol.*, 2019, **4**(7), 1900185.
5 H. Zeng, O. M. Wani, P. Wasylczyk and A. Priimagi, Light-Driven, Caterpillar-Inspired Miniature Inching Robot, *Macromol. Rapid Commun.*, 2018, **39**(1), 1700224.
6 X. Chen, B. Jang, D. Ahmed, C. Hu, C. De Marco and M. Hoop, *et al.*, Small-Scale Machines Driven by External Power Sources, *Adv. Mater.*, 2018, **30**(15), 1705061.
7 M. Li, N. A. Ostrovsky-Snider, M. Sitti and F. G. Omenetto, Cutting the Cord: Progress in Untethered Soft Robotics and Actuators, *MRS Adv.*, 2019, **4**(51–52), 1–18.
8 S. I. Rich, R. J. Wood and C. Majidi, Untethered soft robotics, *Nat. Electron.*, 2018, **1**(2), 102–112.
9 F. N. Piñan Basualdo, A. Bolopion, M. Gauthier and P. Lambert, A microrobotic platform actuated by thermocapillary flows for manipulation at the air-water interface, *Sci. Robot.*, 2021, **6**(52), eabd3557.
10 J. M. K. Ng, M. J. Fuerstman, B. A. Grzybowski, H. A. Stone and G. M. Whitesides, Self-assembly of gears at a fluid/air interface, *J. Am. Chem. Soc.*, 2003, **125**(26), 7948–7958.
11 H. Zhou, C. C. Mayorga-Martinez, S. Pané, L. Zhang and M. Pumera, Magnetically Driven Micro and Nanorobots, *Chem. Rev.*, 2021, **121**(8), 4999–5041.
12 P. Cabanach, A. Pena-Francesch, D. Sheehan, U. Bozuyuk, O. Yasa and S. Borros, *et al.*, Zwitterionic 3D-Printed Non-Immunogenic Stealth Microrobots, *Adv. Mater.*, 2020, **32**(42), 2003013.
13 C. Maggi, F. Saglimbeni, M. Dipalo, F. De Angelis and R. Di Leonardo, Micromotors with asymmetric shape that efficiently convert light into work by thermocapillary effects, *Nat. Commun.*, 2015, **6**, 7855.
14 W. Wang, Y. Liu, Y. Liu, B. Han, H. Wang and D. Han, *et al.*, Direct Laser Writing of Superhydrophobic PDMS Elastomers for Controllable Manipulation via Marangoni Effect, *Adv. Funct. Mater.*, 2017, **27**(44), 1702946.
15 H. Zeng, P. Wasylczyk, C. Parmeggiani, D. Martella, M. Burresi and D. S. Wiersma, Light-Fueled Microscopic Walkers, *Adv. Mater.*, 2015, **27**(26), 3883–3887.
16 M. Zhang, H. Shahsavan, Y. Guo, A. Pena-Francesch, Y. Zhang and M. Sitti, Liquid-Crystal-Elastomer-Actuated Reconfigurable Microscale Kirigami Metastructures, *Adv. Mater.*, 2021, **33**(25), 2008605.

17 T. Qiu, S. Palagi, A. G. Mark, K. Melde, F. Adams and P. Fischer, Wireless actuation with functional acoustic surfaces, *Appl. Phys. Lett.*, 2016, **109**(19), 191602.
18 D. Ahmed, X. Mao, J. Shi, B. K. Juluri and T. J. Huang, A millisecond micromixer via single-bubble-based acoustic streaming, *Lab Chip*, 2009, **9**(18), 2738–2741.
19 A. Aghakhani, O. Yasa, P. Wrede and M. Sitti, Acoustically powered surface-slipping mobile microrobots, *Proc. Natl. Acad. Sci. U. S. A.*, 2020, **117**(7), 3469–3477.
20 Y. Alapan, B. Yigit, O. Beker, A. F. Demirörs and M. Sitti, Shape-encoded dynamic assembly of mobile micromachines, *Nat. Mater.*, 2019, **18**(11), 1244–1251.
21 A. Pena-Francesch, J. Giltinan and M. Sitti, Multifunctional and biodegradable self-propelled protein motors, *Nat. Commun.*, 2019, **10**(1), 3188.
22 J. M. Catchmark, S. Subramanian and A. Sen, Directed rotational motion of microscale objects using interfacial tension gradients continually generated via catalytic reactions, *Small*, 2005, **1**(2), 202–206.
23 J. W. M. Bush and D. L. Hu, WALKING ON WATER: Biolocomotion at the Interface, *Annu. Rev. Fluid Mech.*, 2006, **38**(1), 339–369.
24 E. Lauga and A. M. J. Davis, Viscous Marangoni propulsion, *J. Fluid Mech.*, 2012, **705**, 120–133.
25 B. Kwak, S. Choi, J. Maeng and J. Bae, Marangoni effect inspired robotic self-propulsion over a water surface using a flow-imbibition-powered microfluidic pump, *Sci. Rep.*, 2021, **11**(1), 17469.
26 C. H. Meredith, A. C. Castonguay, Y. J. Chiu, A. M. Brooks, P. G. Moerman and P. Torab, *et al.*, Chemical design of self-propelled Janus droplets, *Matter*, 2022, **5**(2), 616–633.
27 Y. Ikezoe, G. Washino, T. Uemura, S. Kitagawa and H. Matsui, Autonomous motors of a metal–organic framework powered by reorganization of self-assembled peptides at interfaces, *Nat. Mater.*, 2012, **11**(12), 1081–1085.
28 N. Bassik, B. T. Abebe and D. H. Gracias, Solvent Driven Motion of Lithographically Fabricated Gels, *Langmuir*, 2008, **24**(21), 12158–12163.
29 M. L. Timm, S. Jafari Kang, J. P. Rothstein and H. Masoud, A remotely controlled Marangoni surfer, *Bioinspiration Biomimetics*, 2021, **16**(6), 066014.
30 Z. S. Davidson, H. Shahsavan, A. Aghakhani, Y. Guo, L. Hines and Y. Xia, *et al.*, Monolithic shape-programmable dielectric liquid crystal elastomer actuators, *Sci. Adv.*, 2019, **5**(11), eaay0855.
31 M. Rogóż, K. Dradrach, C. Xuan and P. Wasylczyk, A Millimeter-Scale Snail Robot Based on a Light-Powered Liquid Crystal Elastomer Continuous Actuator, *Macromol. Rapid Commun.*, 2019, **40**(16), 1900279.
32 H. Zeng, P. Wasylczyk, D. S. Wiersma and A. Priimagi, Light Robots: Bridging the Gap between Microrobotics and Photomechanics in Soft Materials, *Adv. Mater.*, 2018, **30**(24), 1703554.
33 M. Pilz da Cunha, S. Ambergen, M. G. Debije, E. F. G. A. Homburg, J. M. J. den Toonder and A. P. H. J. Schenning, A Soft Transporter Robot Fueled by Light, *Adv. Sci.*, 2020, **7**(5), 1902842.
34 T. J. White and D. J. Broer, Programmable and adaptive mechanics with liquid crystal polymer networks and elastomers, *Nat. Mater.*, 2015, **14**(11), 1087–1098.
35 L. Dong and Y. Zhao, Photothermally driven liquid crystal polymer actuators, *Mater. Chem. Front.*, 2018, **2**(11), 1932–1943.
36 H. Shahsavan, S. M. Salili, A. Jákli and B. Zhao, Smart Muscle-Driven Self-Cleaning of Biomimetic Microstructures from Liquid Crystal Elastomers, *Adv. Mater.*, 2015, **27**(43), 6828–6833.
37 H. Shahsavan, A. Aghakhani, H. Zeng, Y. Guo, Z. S. Davidson and A. Priimagi, *et al.*, Bioinspired underwater locomotion of light-driven liquid crystal gels, *Proc. Natl. Acad. Sci. U. S. A.*, 2020, **117**(10), 5125–5133.
38 I. Colomer, A. E. R. Chamberlain, M. B. Haughey and T. J. Donohoe, Hexafluoroisopropanol as a highly versatile solvent, *Nat. Rev. Chem.*, 2017, **1**(11), 88.
39 A. Pena-Francesch, S. Florez, H. Jung, A. Sebastian, I. Albert and W. Curtis, *et al.*, Materials Fabrication from Native and Recombinant Thermoplastic Squid Proteins, *Adv. Funct. Mater.*, 2014, **24**(47), 7401–7409.
40 A. Pena-Francesch, N. E. Domeradzka, H. Jung, B. Barbu, M. Vural and Y. Kikuchi, *et al.*, Research Update: Programmable tandem repeat proteins inspired by squid ring teeth, *APL Mater.*, 2018, **6**(1), 10701.
41 A. Pena-Francesch and M. C. Demirel, Squid-Inspired Tandem Repeat Proteins: Functional Fibers and Films, *Front. Chem.*, 2019, **7**, 69.
42 A. Pena-Francesch, H. Jung, M. C. Demirel and M. Sitti, Biosynthetic self-healing materials for soft machines, *Nat. Mater.*, 2020, **19**(11), 1230–1235.
43 L. T. de Haan, C. Sánchez-Somolinos, C. M. W. Bastiaansen, A. P. H. J. Schenning and D. J. Broer, Engineering of Complex Order and the Macroscopic Deformation of Liquid Crystal Polymer Networks, *Angew. Chem.*, 2012, **124**(50), 12637–12640.
44 A. Lebar, G. Cordoyiannis, Z. Kutnjak and B. Zalar, The Isotropic-to-Nematic Conversion in Liquid Crystalline Elastomers. in: W. H. de Jeu, ed., *Liquid Crystal Elastomers: Materials and Applications*, Berlin, Heidelberg: Springer Berlin Heidelberg, 2010. pp. 147–185.

